Engineering Structures 175 (2018) 926–943

Contents lists available at ScienceDirect

Engineering Structures

journal homepage: www.elsevier.com/locate/engstruct

Cross-platform implementation, verification and validation of advanced mathematical models of elastomeric seismic isolation bearings

Manish Kumar*, Andrew S. Whittaker

Department of Civil Engineering, Indian Institute of Technology Bombay, Mumbai, India
Department of Civil, Structural and Environmental Engineering, University at Buffalo, NY, USA

ARTICLE INFO

Keywords:
Elastomeric bearing
Lead rubber
Seismic isolation
Verification
Validation
OpenSees
ABAQUS
LS-DYNA
User elements

ABSTRACT

Stable inelastic response of seismic isolation bearings is key to the successful performance of base isolated nuclear structures, buildings and bridges. Since full-scale isolated nuclear structures (and buildings) cannot be tested for extreme earthquakes on simulators because their payload capacities are orders of magnitude smaller than weights of structures, confirmation of adequate performance must be provided by analysis of numerical models and testing of individual bearings. As the consequences of isolator failure are high, for example, core damage in a nuclear power plant and collapse for a building, the numerical models of the key nonlinear components, namely, the isolators, must be verified and validated (V + V). Herein, advanced models of elastomeric seismic isolation bearings are implemented as user elements in the open-source code OpenSees, and the commercial codes ABAQUS and LS-DYNA. These advanced models are verified and validated following ASME best practice to predict response under extreme loadings. Sources of error in the computational models are quantified, and where possible, eliminated. Those isolator characteristics crucial to robust estimates of performance are identified. Experiments are performed to obtain data for validation. The isolator models are validated using data from experiments and values of model parameters are recommended.

1. Introduction

Analysis of elastomeric bearings for extreme loadings requires robust mathematical models that consider all of the properties that are expected to be critical under such loadings. Mathematical models have been proposed (e.g., [1–3]), including the advanced model of Kumar et al. [4]. These models capture the behaviour of elastomeric bearings with varying degree of sophistication. However, a robust model of elastomeric bearing capable of capturing response associated with extreme earthquake shaking is not available in any of the contemporary codes. The software codes used for the seismic analysis of base-isolated structures, including SAP2000 [5] and PERFORM-3D [6], provide simplified models of elastomeric (and sliding) bearings, as noted in Table 1. Previously, the open-source seismic analysis program OpenSees included more sophisticated isolator models (see Table 1) but could not capture the more complex characteristics described in Kumar et al. [4] (e.g., cavitation, interaction between axial compression and shear stiffness, change in hysteresis due to heating of the lead core).

The finite element programs (LS-DYNA [7] and ABAQUS [8]) can model complex isolator behaviors (see Table 1) using either discrete or continuum approaches. Of these two general-purpose FEA programs, only LS-DYNA provides a direct option to model an isolator based on its material and geometrical properties. The continuum approach is recommended when the behavior of an individual isolator is to be studied. For analysis of large base-isolated structures, the discrete model will generally have to be used. Implementation of a computationally efficient discrete model of an elastomeric bearing is required in multiple codes to enable analysis of the response of base-isolated structures under extreme earthquake shaking.

The credibility, reliability and consistency of advanced models of an elastomeric bearing implemented in different software codes need to be established to ensure confidence in their use. The models developed for the analysis of engineered systems are always approximations of the physical reality and are limited by knowledge of physical processes, available data, mathematical formulations and numerical tools of analysis. The degree of accuracy to which these models predict the response of a system is addressed by the process of Verification and Validation (V + V). The prediction of response of a physical event through engineering models consists of many steps, and each step is accompanied by sources of error. The magnitude of the error depends on the assumptions, tools and techniques used for the analysis. Mathematical models should always be verified and validated (V + V).

* Corresponding author at: Department of Civil Engineering, Indian Institute of Technology Bombay, Mumbai 400076, India.
E-mail address: mkumar@iitb.ac.in (M. Kumar).

https://doi.org/10.1016/j.engstruct.2018.08.047
Received 22 December 2017; Received in revised form 13 August 2018; Accepted 17 August 2018
Available online 03 September 2018
0141-0296/

Table 1
Modeling of elastomeric seismic isolators and software programs.

Properties	SAP2000	PERFORM3D	LS-DYNA	ABAQUS	OpenSees
Coupled horizontal directions	Yes	Yes	Yes	Yes	Yes
Coupled horizontal and vertical directions	No	No	No	No	No
Different tensile and compressive stiffness	No	Yes	Yes	Yes	Yes
Nonlinear tensile behavior	No	No	No	Yes	Yes
Cavitation and post-cavitation	No	No	No	No	No
Nonlinear compressive behavior	No	No	No	Yes	Yes
Varying buckling capacity	No	No	No	No	No
Heating of lead core	No	No	No	No	No

There is much literature that provide qualitative and quantitative guidelines on V + V (e.g., ASME [9] Oberkampf and Roy [10], Oberkampf et al. [11], Thacker et al. [12], Roache [13]) but these are focused towards mechanical and aerospace applications. Formal V + V is still not implemented for models in structural and earthquake engineering applications, where large-scale nonlinear systems are modeled with high uncertainty and variability in material and mechanical properties. The V + V for structural models is mostly limited to code-to-code verification. Here-in, an advanced model of an elastomeric bearing is V + V: the first such application in structural and earthquake engineering to a highly nonlinear component of a structure. Lack of examples is also an impediment to widespread adoption of formal V + V for structural and earthquake engineering applications. A presentation on how V + V of nonlinear numerical models of structural engineering components should be performed, including a formal treatment of sources and magnitudes of error is needed, and that is also presented in this paper.

The system of interest here is an isolation system for a building or a nuclear power plant (NPP), and includes models of low damping rubber (LDR) and lead-rubber (LR) bearings. Seismic isolation is used to protect mission-critical infrastructure from the effects of horizontal earthquake shaking. Mainstream seismic isolators in the United States are elastomeric bearings (with and without a central lead core) and spherical sliding bearings. These bearings are typically installed at the base of the structure, above a foundation and below a basemat. Fig. 1 presents a cut-away view of a seismically isolated NPP. In this view, the isolators are shown installed atop pedestals. The isolators are vertically stiff and horizontally flexible, providing isolation in the horizontal direction only. Fig. 2 is a cut-away view of a lead-rubber bearing: an elastomeric bearing constructed with alternating layers of natural rubber and steel shims, with a central lead plug to provide energy dissipation (damping).

2. Motivation

The stable inelastic response of seismic isolation bearings such as that shown in Fig. 2 is key to the successful performance of base-isolated nuclear structures (and buildings). Such structures are designed for earthquake shaking with return periods of between 2500 years (buildings) and 100,000 years (nuclear power plants). Since full-size isolated nuclear structures (and buildings) cannot be tested for extreme earthquakes on simulators because their maximum payloads are orders of magnitude smaller than the weights of buildings (1000 s of tons) and nuclear structures (100,000 s of tons), and maximum actuator displacements and velocities are smaller than those needed to simulate extreme earthquake shaking, confirmation of adequate performance must be provided by a combination of analysis of numerical models and dynamic testing of prototype bearings. Since the consequences of failure are extremely high, for example, core damage in a nuclear power plant and collapse for a building, the numerical models of the key nonlinear components in the structure, namely, the isolators, must be verified and validated (V + V).

Prior to the work described in this paper, there were no numerical models of elastomeric seismic isolators available in any finite element code capable of capturing all of the responses identified in the first column of Table 1. This paper describes the implementation of advanced user elements/materials in the open-source code OpenSees and in the commercial codes ABAQUS and LS-DYNA. Relevant information on V + V is presented. Models of elastomeric bearings are described and a V + V plan is developed and implemented for them. Modeling errors due to different sources are quantified and either minimized or eliminated. These V + V activities help an analyst establish confidence in the models and be aware of possible errors in calculated responses.

3. Background

The V + V process starts with the definition of the domain of interest, which is the physical system and associated environment for which the model is to be created. A conceptual model of the physical problem is formulated through a set of features that are expected to play a role in the physical event for which the model is to be used. A mechanics-based representation of the physical problem that is amenable to mathematical and computational modeling is created, which includes: (1) geometrical details of the model, (2) material definition, (3) initial and boundary conditions, (4) external loads, and (5) modeling and analysis approach. A mathematical description of the conceptual model is formulated through a set of equations and statements that describe the physical problem. The mathematical model uses parameters that are one of the major sources of uncertainty that affects its accuracy. A computational model is developed using the mathematical model to predict the system's response. The process involves spatial and temporal discretization of the mathematical model into a numerical model and its implementation in a computer program using an algorithm that solves the model through direct or iterative solution techniques. Domain discretization and solution techniques are the major sources of the error in the computational model; round-off errors and coding bugs are other sources. The process of model development and V + V plan is summarized in Fig. 3.

Verification addresses the accurate representation of a mathematical model through software implementation of a numerical model; a relationship to the physical reality is not of concern. Validation addresses the degree of accuracy to which the mathematical model represents the physical reality, which is represented by experimental data. ASME [9] provides a list of standard terms used in V + V. It defines verification and validation as:

Verification: The process of determining that a computational model accurately represents the underlying mathematical model and its solution.

Validation: The process of determining the degree to which a model is an accurate representation of the real world from the perspective of the intended uses of the model.

Verification activities are performed to improve the accuracy of the computational results. The system response obtained from analysis of verified models is compared with data obtained from validation

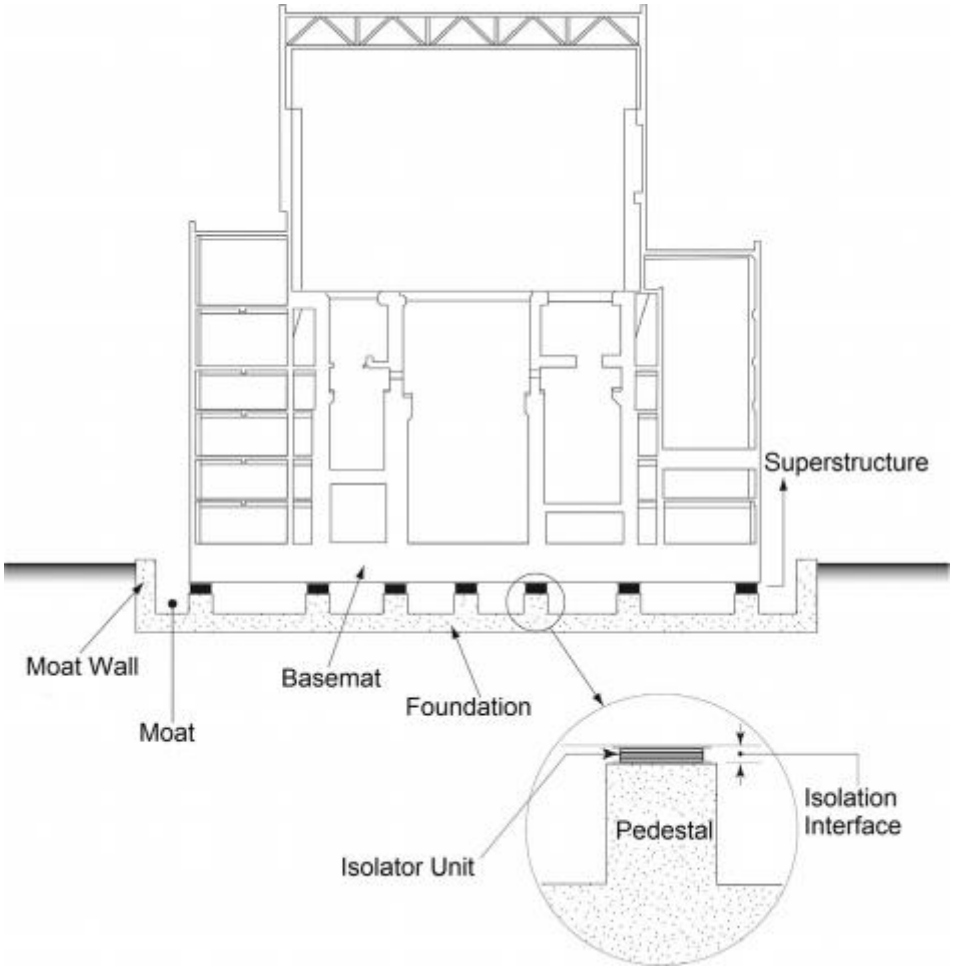

Fig. 1. Cut-away view of a base-isolated NPP [14].

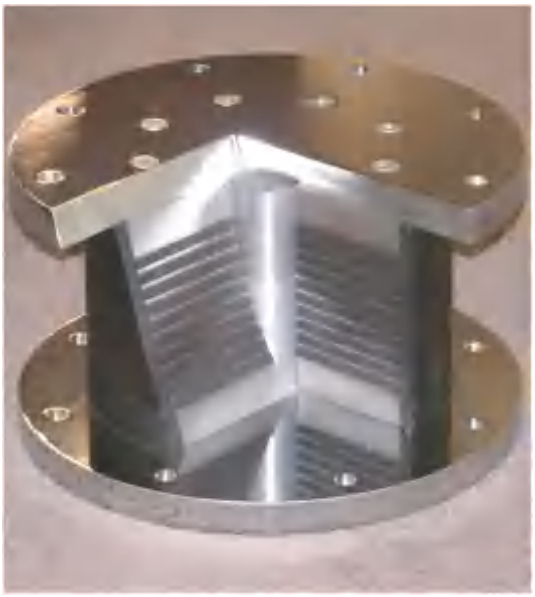

Fig. 2. Lead-rubber isolator [15].

experiments. The test data must be processed to remove measurement errors. If the computational results are within tolerance per an established accuracy criterion, the model is deemed validated. If not, the model needs to be revised.

4. Model development

The models of LDR and LR bearings from Kumar et al. [4] are summarized here. The physical model of an elastomeric bearing is formulated as a two node, twelve-degree of freedom element. The two nodes are connected by six springs, which represent the material models in the six basic directions. The six material models capture the behavior in the axial, shear (2), torsional and rotational (2) directions. The conceptual model and physical model of the LR bearing of Fig. 2 are shown in Fig. 4a and b, respectively. The hierarchy of the mathematical model and its components are shown in Fig. 5.

A detailed discussion on the materials models in the six basic directions is presented in Kumar et al. [4]. The two-spring model [16], validated by Warn et al. [17], is used to model behavior in axial compression. The compressive stiffness, K_v, and the buckling load, P_{cr}, depend on the lateral displacement, u_h.

Linear response in tension, with stiffness equal to K_v, is assumed up to cavitation. The initial cavitation force in an elastomeric bearing is calculated as $F_c = 3GA$, where A is the bonded rubber area before cavitation, and the shear modulus, G, is obtained from testing at moderate shear strains under nominal axial loads.

The post-cavitation force, F, at tensile displacement u is described by the relationship:

$$F(u) = F_c\left[1 + \frac{1}{kT_r}(1-e^{-k(u-u_c)})\right] \quad (1)$$

where u_c is the initial cavitation displacement, calculated by dividing F_c by K_{v0}; k is a parameter that describes the post-cavitation variation of

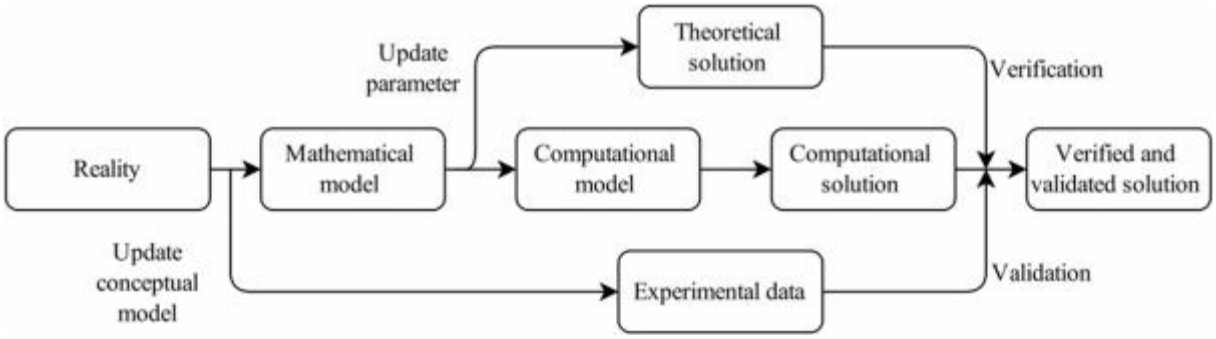

Fig. 3. Verification, validation and model calibration plan for elastomeric bearings.

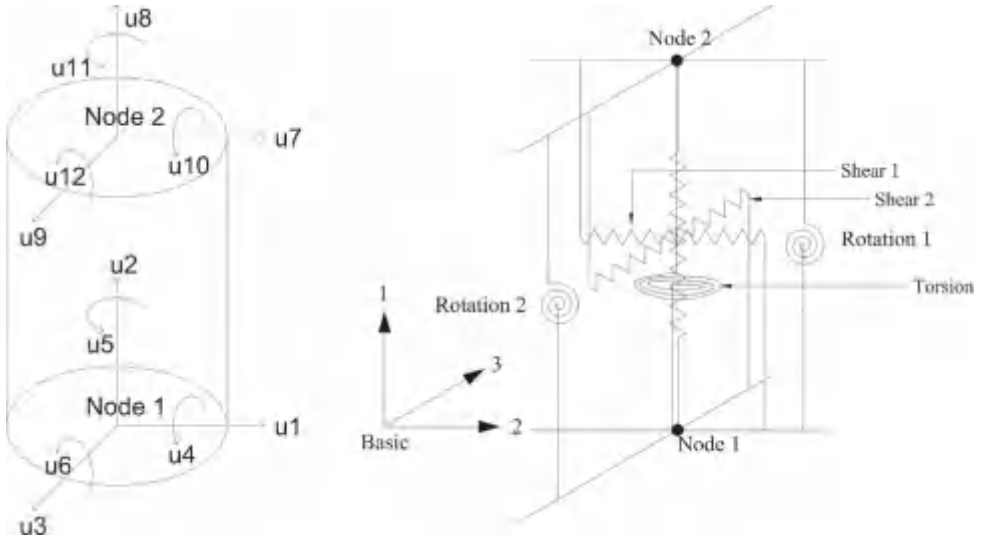

a) Conceptual model b) Physical model

Fig. 4. Models of a LR bearing.

tensile stiffness; T_r is the total rubber thickness; and other terms are defined above.

The damage under the cyclic tensile loading is modeled using the state variable, u_{max}, which is the maximum tensile deformation. A damage index ϕ is defined:

$$\phi = \phi_{max}\left[1-\exp\left(-a\left(\frac{u-u_c}{u_c}\right)\right)\right] \quad (2)$$

where a defines the rate of damage, ϕ_{max} is the maximum damage that can be expected in a bearing, and other terms are defined above. The reduced cavitation force and displacement (F_{cn}, u_{cn}) in subsequent cycles are calculated using the damage index. Fig. 6a presents the mathematical model of an elastomeric bearing in the axial direction. The model requires the user to assign values to three parameters: k, a, and ϕ_{max}.

The behavior in the horizontal direction is represented by the Bouc-Wen model [18,19] extended for analysis of seismic isolators under bidirectional horizontal motion by Nagarajaiah et al. [20]. The loss of strength in a LR bearing due to heating of its lead core is incorporated using the model proposed by Kalpakidis et al. [21]. The mathematical model of an elastomeric bearing in shear is presented in Fig. 6b.

5. Model implementation

The mathematical model of an elastomeric bearing is implemented as user elements (UELs) in OpenSees and ABAQUS, and as a user material (UMAT) in LS-DYNA.[1]. A user element is an implementation of a numerical model in a computer program using a programming language. Two elements are created in each program for LDR and LR bearings. The new user material for the LR bearing enables modeling of the following mechanical characteristics or behaviors:

1. Strength degradation in shear due to heating of the lead core (LR bearings)
2. Variation in buckling load due to horizontal displacement
3. Cavitation and post-cavitation behavior due to tensile loading
4. Variation in axial stiffness due to horizontal displacement
5. Variation in shear stiffness due to axial load

These user elements or materials work on similar principles. The nodal force vector and the stiffness-matrix calculations are performed by these elements and transformed from local to global coordinate systems, which are the element's contribution to the global force and stiffness matrices. These elements can be used in three type of analysis, namely: (1) eigenvalue (modal) analysis, (2) static analysis, and (3) transient (dynamic) analysis. The UMAT in LS-DYNA is limited to explicit analysis and cannot be used to perform modal analysis that makes use of implicit methods.

[1] Unless noted otherwise, all UELs and UMATs are referred to as isolator elements hereafter.

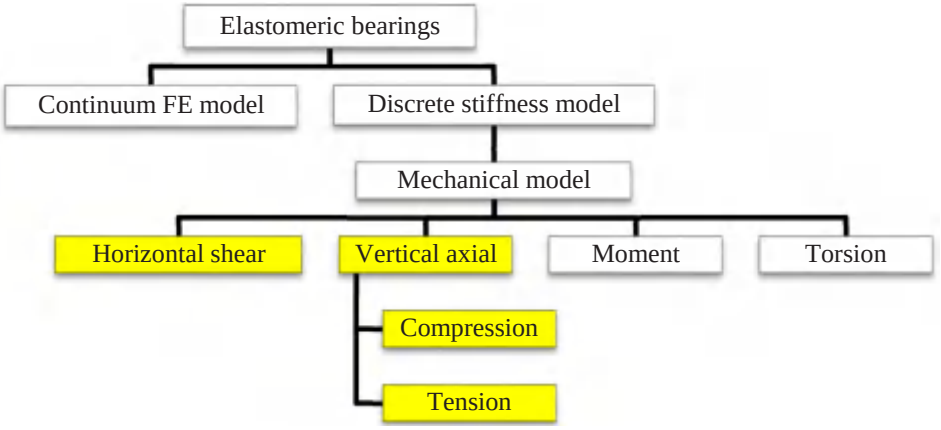

Fig. 5. Hierarchy of the model for an elastomeric bearing.

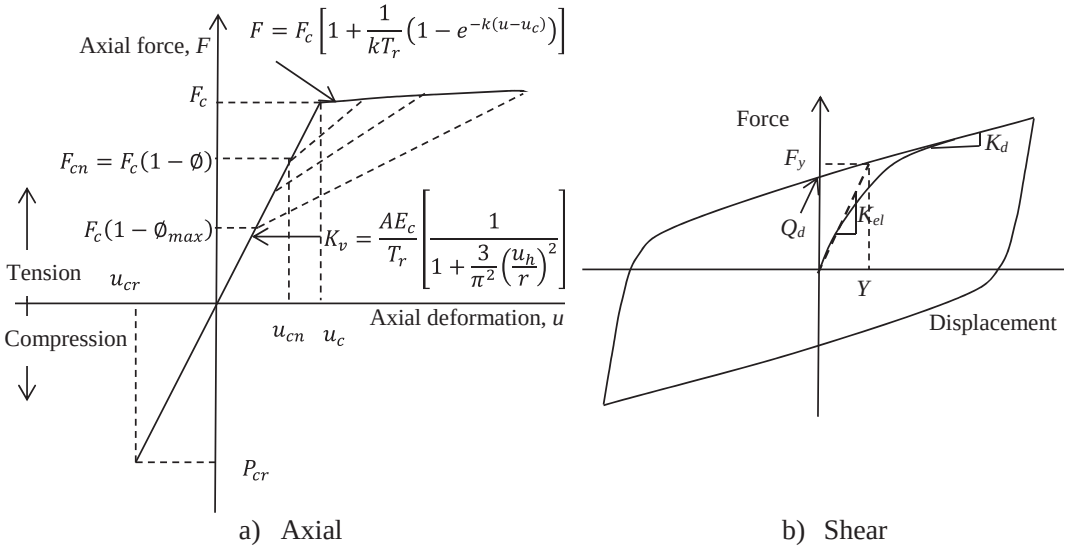

Fig. 6. Advanced models of an elastomeric bearing.

5.1. User elements in OpenSees

The Open System for Earthquake Engineering Simulation (OpenSees) is an object-oriented, open-source software framework for simulations in earthquake engineering using finite element methods. OpenSees has a modular architecture that allows users to add functionality without much dependence on other components of the program. Two elements, ElastomericX and LeadRubberX, were created for LDR and LR bearings, respectively. Both element classes use a similar structure and input arguments. These elements can only be used with three-dimensional finite element models in OpenSees. The elements take basic geometric and material parameters of elastomeric bearings as input arguments. Input arguments include mandatory and optional parameters. Default values of the optional arguments are provided in the element.

5.2. User elements in ABAQUS

Two user subroutines (i.e., UELs) were created: ElastomericX for the LDR bearing and LeadRubberX for the LR bearing. The LeadRubberX element builds on the formulation of ElastomericX and adds thermo-mechanical properties to capture strength degradation due to heating of the lead core.

The response of a system modeled in ABAQUS is obtained by solution of equilibrium equations in incremental steps using the Newton-Raphson method. User elements are coded to define its contribution to the model of the entire structure. The user element is called when element calculations are required. Analysis calculations in ABAQUS are performed using three arrays: (1) RHS, (2) AMATRX, and (3) SVARS. The RHS is an array containing contributions of the element to the right hand side vector (residual force) of the overall system of equations and AMATRX is the array containing the contributions of the element to the Jacobian (stiffness) of the overall system of equations. The SVARS vectors contains values of solution-dependent state variables (e.g., displacements, accelerations, temperature). The primary tasks of user elements are to provide the RHS and AMATRX arrays during the analysis step and to update the SVARS array. The user can specify any arbitrary length of the element, however a length representative of the actual height of the elastomeric bearing is recommended. ABAQUS does not store a history of internal parameters between steps. Solution-dependent state variables must be defined to store parameter values that are required for calculations at the next step. This is done through storing solution-dependent state variables in SVARS and updating them at the end of each step. Twenty-seven and twenty-eight state variables are defined in ElastomericX and LeadRubberX, respectively, with LeadRubberX containing an extra variable to store the temperature of the lead core.

The programming structure of the UEL subroutine is shown in Fig. 7. The main body of executable statements, which consists of set of tasks that need to be performed for each analysis case, is supplemented

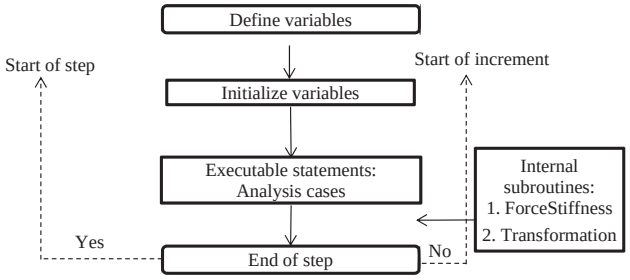

Fig. 7. Programming structure of user elements (adapted from Dassault [22]).

by two internal user subroutines: (1) ForceStiffness – to calculate the nodal force and stiffness matrices of the element in global coordinates, and (2) Transformation – to transform the quantities from one coordinate system to another.

5.3. User material in LS-DYNA

LS-DYNA provides a direct option to model seismic isolators through a material model option ∗MAT_SEISMIC_ISOLATOR [23]. The corresponding element and section is created using options ∗ELEMENT_BEAM and ∗SECTION_BEAM, respectively. ELFORM is set to 6 (discrete beam) and the local axes of the isolator are defined in the ∗SECTION_BEAM option. This material can be used to model elastomeric bearings, flat sliding bearings, single concave Friction Pendulum™ (FP) bearings, double concave FP bearings, and tension-restrained FP bearings. A new material option for LR bearings is created in LS-DYNA to implement the advanced numerical model of an elastomeric seismic isolation bearing described in the preceding sections. It is available as the third option (ITYPE = 3) in ∗MAT_SEISMIC_ISOLATOR, the other two options being Friction Pendulum bearing (ITYPE = 0, 2) and elastomeric bearing (ITYPE = 1).

5.4. Verification criteria

The scope of a model and its intended use must be defined for V + V activities, which helps to prioritize tasks and allocate resources for each activity. Table 2 presents the information required to begin the V + V process.

The components of a mathematical model that need to be verified and validated are selected based on their importance to the response quantities of interest. For example, rotational and torsional behaviors of individual isolators do not contribute to the global rotational and torsional response of an isolated building, which depends purely on the shear and axial behaviors of isolators. Therefore, V + V tasks are performed only for the mechanical behavior of the LDR and LR bearings in the horizontal shear and the vertical axial directions, as identified by the highlighted text in Fig. 5.

Table 2
Scope of V + V for the models of elastomeric bearings.

Feature	Description
Domain of interest	Seismic isolation of buildings, including NPPs
Intended use of the model	Response-history analysis for design- and beyond-design-basis earthquake loadings
Response features of interest	1) Acceleration, velocity, displacement a) of the structure b) of secondary systems and components 2) force and displacement in the isolators 3) energy dissipation (damping) in the isolators a) due to heating in the lead core of LR bearings b) due to cavitation under tension
Accuracy requirements	Must be decided after consultation with stakeholders

Table 3
Phenomena ranking and identification table for models of elastomeric bearings.

Phenomenon	Importance to response of interest	Level of confidence in model
Coupled horizontal directions	High	High
Heating of lead core in LR bearing	High	High
Varying buckling capacity	High	Medium
Coupled horizontal and vertical response	Medium	Medium
Nonlinear tensile behavior	Medium	Low
Cavitation and post-cavitation	Medium	Low
Nonlinear compressive behavior	Low	Low
Post-buckling behavior	Low	Low

The features that are expected to have significant effects on the response of a base-isolated building are identified by constructing a Phenomena Identification and Ranking Table (PIRT). The PIRT for the models of elastomeric bearings is presented in Table 3. The confidence and importance levels assigned to the different components of the mathematical model in Table 3 are based on preliminary information available on the mathematical models of elastomeric bearings and the results of response-history analysis of a seismically isolated NPP [24].

The PIRT helps prioritize those physical characteristics that should be investigated experimentally for validation. If the outcome of V + V points towards a different priority order from the initial assumption, an iteration is performed. Phenomena with medium or high importance to response quantities of interest and low level of confidence in modeling are assigned high priority.

Heating of the lead core and coupling effects are assigned a low priority for validation as they are based on robust mechanical formulations and have already been validated under similar conditions [17,25]. The two-spring model by Koh and Kelly [16] describes the elastic behavior of elastomeric bearing in the vertical direction and can be used with high confidence. The model for the variation in the buckling load capacity with lateral displacement is expected to be of high importance.

Buckling is modeled using the linear approximation of the area-reduction method, which is numerically robust and has been validated experimentally [26]. Robustness is achieved in a numerical sense by sacrificing some of the accuracy in the area-reduction method. Accordingly, this has been assigned a medium level of confidence.

The phenomenological model of Kumar et al. [4] is used for cavitation, post-cavitation and strength reduction in cyclic tension. Cavitation may occur in the bearings around the perimeter of the isolation system due to rocking and/or vertical excitation. Cavitation in individual bearings will not affect the horizontal or vertical response of the superstructure, which will depend on the behavior of the isolation system. The parameters of the phenomenological model are obtained from test data. The uncertainty associated with these parameters is high and so a low confidence of modeling is assigned in Table 3. The effect of cavitation and post-cavitation behavior on system response is not known a priori but is expected to be of medium importance to the response quantities of interest. Phenomena with medium or high importance to response quantities of interest and low level of confidence in modeling are given high priority for the experimental validation activities. The phenomenological model that describes the behavior of an elastomeric bearing in cyclic tension is validated experimentally. The parameters associated with cavitation and strength reduction in cyclic tension are estimated.

The accuracy of a model during V + V is measured using the percentage difference between the peak responses, which is better correlated to the performance of structural systems than the cumulative difference over a response history. A computational solution is compared against a reference solution, which, in the case of verification,

can be an exact or a high order estimate of the exact solution, and in validation, must be test data. Cumulative difference norms are also required for some of the verification tests. The L_1 difference norm over a discretized domain provides an average value of absolute difference and is given as:

$$\xi_1 = \frac{1}{N}\sum_{i=1}^{N} |f_{2i} - f_{1i}| \quad (3)$$

The L_2 (Euclidean) norm provides the root mean square of difference over the domain:

$$\xi_2 = \sqrt{\frac{1}{N}\sum_{i=1}^{N} (f_{2i} - f_{1i})^2} \quad (4)$$

where f_{1i} and f_{2i} are the reference solution and the solution for the response quantity of interest, respectively, at the ith sample point, and N is the total number of sample points. The L_1 norm is appropriate when the response quantities contain several discontinuities and singularities in their domain [10]. The L_1 and L_2 norms of error are used here.

6. Verification

6.1. Introduction

Verification of a model is performed to assess the accuracy with which the computational model represents the mathematical model. A model must be verified before it can be used for any validation activity. The errors associated with the computational model should be separated from those arising from use of an inadequate mathematical model that are addressed through validation. The error associated with the unverified computational model might contribute to the value of an unknown parameter determined by calibration. The predicted response of a system will be biased when such parameters are used.

Verification can be categorized as: (1) code verification, and (2) solution verification. Code verification deals with the programming aspects of the computational model and checks whether the discretized numerical model is implemented correctly in the computer program. Solution verification checks for the discretization, iterative convergence, and round-off error.

6.2. Models used for verification

The verification activities are performed using the two-node macro model shown in Fig. 8. All six degrees of freedom of the bottom node (node 1) are fixed to the ground, as are the three rotational degrees of freedom at the top node. The two nodes are joined by the isolator element. The properties of the LDR5 in Warn [27] and larger size LR bearing in Kalpakidis et al. [21] are used for the elements. The properties of the two bearings are presented in Table 4.

The isolated period of the model is a function of the supported weight, W, which is calculated assuming a pressure on the bonded rubber area of the bearing. The weight is divided by g to obtain the corresponding mass, which is lumped in the three translational directions at node 2 for static and dynamic analyses. Two values of pressure were used for the V + V activities. A pressure of 3 MPa, which is typical of service (i.e., dead and live) loadings in the United States, is used for

Fig. 8. Two-node macro model of a base-isolated NPP.

Table 4
Geometrical and mechanical properties of elastomeric bearings.

Property	Notations (units)	Value	
		LDR	LR
Single rubber layer thickness	t_r (mm)	3	9.53
Number of rubber layers	n	20	16
Steel shim thickness	t_s (mm)	3	4.76
Outer diameter	D_o (mm)	152	508
Inner/lead core diameter	D_i (mm)	30	139.7
Rubber cover thickness	t_c (mm)	12	12.7
Shear modulus	G (MPa)	0.80	0.87
Bulk modulus of rubber	K_{bulk}(MPa)	2000	2000
Dynamic yield stress of lead	σ_L (MPa)	n.a.*	13
Total rubber thickness	T_r (mm)	60	152.4

* n.a.: not applicable.

all of the verification studies bar one. A pressure of 7.29 MPa is used for the LR bearing earthquake response study of Section 6.3.2.5 to achieve a target isolation period. This higher pressure is typical of values used in the United States for transient earthquake loadings and was adopted for tests (e.g., [21,27]) that provided data for the validation study of Section 7.3 (see Fig. 30).

The vertical (axial) force-displacement relationship for the model is described in Fig. 6a. The values of axial stiffness in compression and tension are assumed to be identical and equal to K_v. Fig. 6b presents the horizontal (shear) force-displacement relationship, where K_{el} is the initial elastic stiffness, K_d is the post-elastic stiffness, Q_d is the characteristic strength (or zero-displacement force intercept) and Y is the yield displacement. Table 5 lists the values assigned to the LDR and LR models used for the verification studies described in this section. For the LR bearing, $Q_{d,}$ is calculated as the product of the dynamic yield stress of lead and the area of the lead core, and the (small) contribution from the rubber is ignored. The characteristic strength of the LDR bearing is determined using $Q_d = (\pi/2) \times \beta_{eff} \times K_d \times D$, per Kumar et al. [4], where β_{eff} is the equivalent viscous damping ratio in the horizontal direction and D is the horizontal displacement. The value of Q_d for the LDR bearing is calculated assuming a damping ratio of 3% and a horizontal displacement corresponding to 100% shear strain ($D = T_r$) in the rubber. For these LDR and LR bearings, Q_d/W equals 0.013 and 0.336 (0.138), respectively, where 0.013 and 0.336 are calculated assuming a pressure of 3 MPa, and 0.138 is calculated assuming a pressure of 7.29 MPa.

The verification model is a discrete representation (i.e., not a continuum) of an elastomeric bearing. Hence, verification activities are performed using a temporal domain discretization and no spatial discretization is involved.

All verification activities are performed using the ElastomericX and LeadRubberX user elements in OpenSees. The scope of verification for the isolator models in ABAQUS and LS-DYNA is limited to a

Table 5
LDR and LR bearing model parameters.

Property	Notation (units)	Value	
		LDR	LR
Elastic stiffness	K_{el} (kN/mm)	0.426	29.594
Post-elastic stiffness	K_d (kN/mm)	0.272	1.128
Characteristic strength	Q_d (kN)	0.77	199.3
Yield displacement	Y (mm)	5	7
Axial stiffness	K_v (mm)	95.2	516.6
Weight	W (kN)	61[a]	593[a], 1441[b]
Critical buckling load	P_{cr0} (kN)	385	5902
Cavitation force	F_c (kN)	49	516

[a] Corresponds to a pressure of 3 MPa.
[b] Corresponds to a pressure of 7.29 MPa.

comprehensive code-to-code verification.

6.3. Code verification

Code verification assesses the mathematical correctness and implementation of the numerical algorithms in a source code using a programming language. It ensures that the solution algorithms are implemented correctly in the source code and are functioning as intended. Three techniques are employed here for numerical code verification: (1) symmetry test, (2) code-to-code comparison, and (3) order-of-accuracy test.

6.3.1. Symmetry test

The symmetry test is based on the principal that if a computational model is provided with symmetric geometry, initial conditions and boundary conditions, the response should be identical. The elastomeric bearing model is circular and has radial symmetry. The model in OpenSees [28] is subjected to two symmetry conditions: (1) the bearing is fixed at its base and ground motion is applied to the free node at its top in the x-direction, and (2) the bearing is fixed at its top and ground motion applied to the free node at its bottom in the negative x-direction.

Sinusoidal displacement of $T_r \sin(2\pi t/T)$, where T_r is the total rubber thickness and T (= 10 s) is the period of the harmonic excitation, is applied at the free node of the LDR and LR bearing for the two analysis cases. The analysis cases and the results of the symmetry test are presented in Figs. 9 and 10, respectively. The L_1 and L_2 norm of the percentage difference is 0% at a time-step of 0.1 s for the ElastomericX and the LeadRubberX elements.

6.3.2. Code-to-code comparison

Code-to-code comparison is the most widely used verification method to establish confidence in a code implementing a mathematical model. The two prerequisites for code-to-code comparison are [29]: (1) the two codes should implement the same mathematical model, and (2) one of the codes should have undergone rigorous code verification activities. The mathematical model is implemented in OpenSees, ABAQUS and LS-DYNA. Software quality assurance for ABAQUS is provided by a verification manual [30] and a benchmarks manual [31]. Elements of LS-DYNA are NQA-1 compliant [32].

6.3.2.1. Modal analysis. The periods of the two-node macro model in the horizontal and vertical directions are obtained using OpenSees, ABAQUS and LS-DYNA, and these are compared with theoretical values. In the horizontal direction, time periods are calculated based on elastic and post-elastic stiffness. The period obtained using the post-elastic stiffness is the isolation period. Modal analysis in LS-DYNA can only be performed using the implicit method but the UMAT for LR bearings is not available for it. Hence, an indirect approach is used to obtain modal frequencies wherein the two-node macro model is subjected to initial displacements (1 mm) in the horizontal and vertical directions. Time periods are calculated from the free vibration responses presented in Fig. 11.

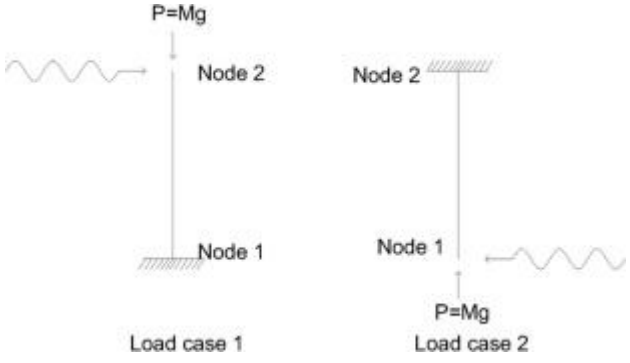

Fig. 9. Analysis cases for the symmetry test of the models of elastomeric bearings.

The time periods of the two-node macro model obtained using first principles calculations, OpenSees, ABAQUS and LS-DYNA are presented in Table 6.

6.3.2.2. Harmonic loading. The large size bearing in Kalpakidis et al. [21] is subjected to displacement-controlled sinusoidal and incremented triangular loading in the horizontal and the vertical directions, respectively. Positive vertical force and displacement are tensile. The responses along the two directions are plotted in Fig. 12. No significant difference is observed between the responses obtained using the isolator elements in OpenSees, ABAQUS and LS-DYNA.

6.3.2.3. Damping calculations. Three damping formulations are investigated here: (1) Rayleigh, (2) mass-proportional, and (3) stiffness-proportional. Modal damping can be implemented in OpenSees [33]. LS-DYNA does not accommodate modal damping and stiffness-proportional damping cannot be applied to discrete elements [23]. ABAQUS does not enable any of three formulations to be used with a user subroutine. Hence, the damping formulations for the isolator user elements are not investigated here.

Analyses are performed to verify damping calculations performed by OpenSees and LS-DYNA. The LR bearing of Kalpakidis et al. [21] is assigned 2% damping in the horizontal direction using the three damping formulations. An initial displacement of 0.01 mm is imposed and the bearing is then allowed to vibrate freely. The analysis is repeated in the axial direction. A small initial displacement is used to ensure linear elastic behavior and avoid any hysteretic damping per Fig. 6b.

The free-vibration displacement response of a single-degree-of-freedom system is:

$$u(t) = e^{-\xi\omega_n t}\left[u(0)\cos\omega_D t + \frac{\dot{u}(0) + \xi\omega_n u(0)}{\omega_D}\sin\omega_D t\right] \quad (5)$$

where ξ is the damping ratio; $u(0)$and $\dot{u}(0)$are the initial displacement and velocity, respectively; ω_n is the natural frequency; and $\omega_D = \omega_n\sqrt{1-\xi^2}$.

The numerical responses of the two-node macro model for the three damping formulations and the analytical responses are presented in Figs. 13 and 14. The damping in the numerical response is calculated using the logarithmic decrement method and values are presented in Table 7. No difference is observed between the assigned damping and the damping calculated from the numerical response using OpenSees. Because LS-DYNA does not enable stiffness-proportional damping, mass-proportional damping is assigned to its isolator element. (An alternative is to use the ∗DAMPING_FREQUENCY_RANGE option that uniformly damps all modes between a defined frequency range. This method is accurate for small values of critical damping ratio.)

6.3.2.4. Moment calculations. The effects of geometric nonlinearity are addressed in the isolator elements using analytical expressions for mechanical properties (e.g., stiffness, buckling load). The nodal moments are obtained using simplified P-Δ calculations. The isolator elements in all three software programs provide an option to distribute the P-Δ moments between the two nodes of the bearing.

To verify the P-Δ calculations, the two-node macro model is modeled using isolator elements in the three programs. Two elements in OpenSees (elastomericBoucWen and TwoNodeLink) are used to verify calculations. Results are compared with theoretical calculations. A horizontal strain of 100% and an axial load equal to 10% of the critical buckling load are applied to the upper node (Node 2) of the macro model. The distribution of the bending moment at the two nodes of the

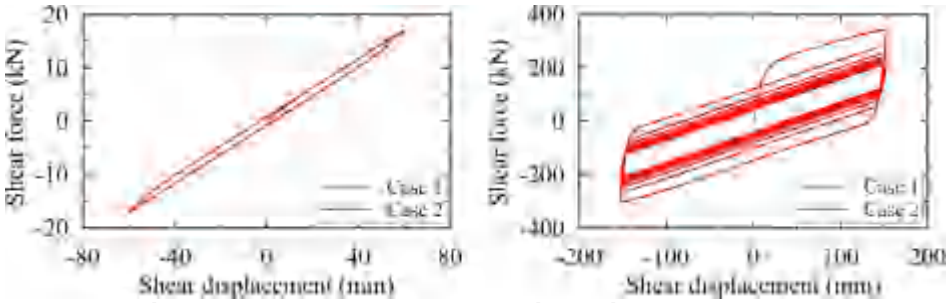

a) LDR bearing, $u = 60sin(0.2\pi t)$ mm b) LR bearing, $u = 152.4sin(0.2\pi t)$ mm

Fig. 10. Symmetry test for models of elastomeric bearings, $\Delta t = 0.1$ sec.

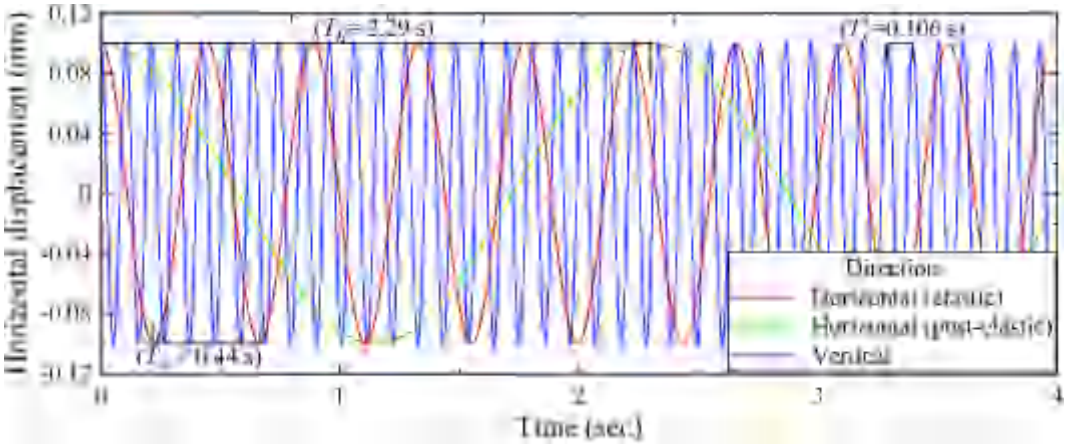

Fig. 11. Free vibration response of the LS-DYNA two-node macro model.

Table 6
Time periods of the two-node macro models (seconds).

Direction	Method of calculation			
	Theory	OpenSees	ABAQUS	LS-DYNA
Horizontal (elastic)	0.443	0.442	0.441	0.441
Horizontal (post-elastic)	2.270	2.269	2.268	2.290
Vertical	0.106	0.106	0.106	0.106

element is shown in Fig. 15. The properties of the LR bearing in Kalpakidis et al. [21] are used for the user elements. The values of parameters F, P, Δ, and h are 371188 N, 590156 N, 0.1524 m, and 0.2238 m, respectively. The theoretical end moment is obtained as $M = (Fh/2 + P\Delta/2)$. The force and the moments at the two nodes of the elastomeric bearing are compared in Table 8. The moments obtained using the isolator elements agree well with the theoretical value except for the isolator element in LS-DYNA that is modeled as pin jointed at its nodes to enable inclusion in the LS-DYNA family of isolator elements, which assumes pin-jointed connectivity. The moment output by LS-DYNA is due only to the vertical load. (The pin-jointed connectivity of the LS-DYNA model has no practical effect on calculated responses because the rotational and torsional stiffness of individual isolators do not contribute meaningfully to the global stiffness of the isolated structure. For design, the analyst can add the moment induced by shear, time step by time step, to the moment output by LS-DYNA.)

6.3.2.5. Earthquake excitation. The two-node macro model of the LR bearing of Tables 4 and 5 is subjected to three-dimensional ground motion excitation and response is calculated using OpenSees, ABAQUS and LS-DYNA. The Newmark implicit integrator ($\Delta t = 0.005$ s) is used in OpenSees and ABAQUS; calculations are performed using the explicit method in LS-DYNA. The three-components of NGA 72 (Lake Hughes, 1971 San Fernando earthquake) are spectrally matched to the uniform hazard response spectra for design-basis earthquake shaking at the site of the Diablo Canyon Nuclear Generating Station; see Kumar et al. [34] for details. The spectrally matched acceleration histories and the corresponding spectra are presented in Fig. 16. Rayleigh damping of

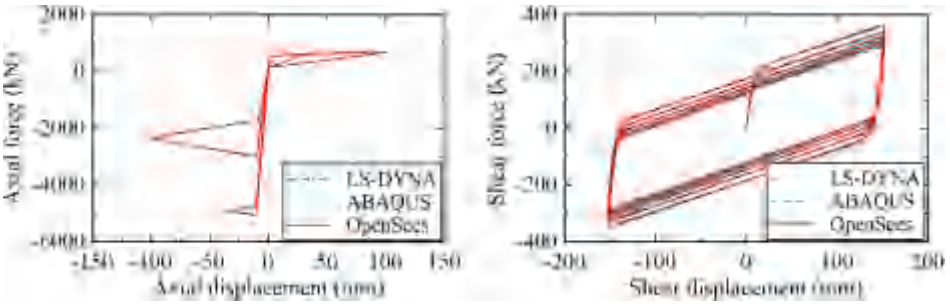

a) Horizontal (shear), $u = 152.4sin(\pi t)$ mm b) Vertical (axial)

Fig. 12. Code-to-code comparisons for displacement-controlled inputs.

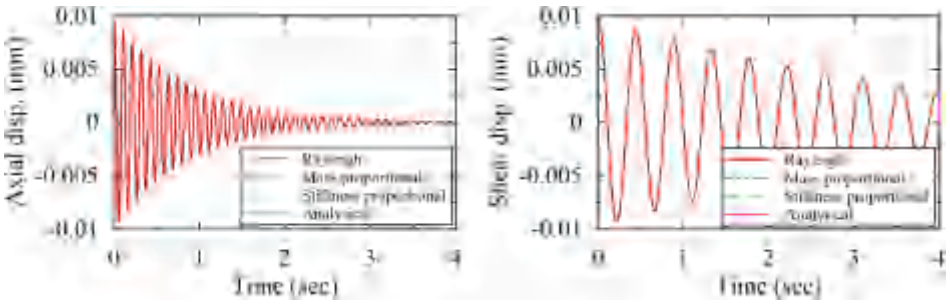

a) Axial b) Shear

Fig. 13. Free vibration response of a LR bearing using OpenSees, u_o = 0.01 mm, ζ = 2%.

2% is assigned based on the horizontal isolation frequency and vertical axial frequency, providing all the damping in the vertical direction (rubber only), and supplementing the hysteretic damping in the horizontal direction (lead core).

The peak forces and displacements obtained using the isolator elements in OpenSees, ABAQUS and LS-DYNA are presented in Tables 9 and 10, respectively. In these tables, positive forces and displacements in the Z direction are tensile. Responses are reported for three cases: (1) no vertical excitation, (2) 25% vertical excitation, and (3) 100% vertical excitation, where 100% excitation is described by the Z-direction spectrum in Fig. 16b. Figs. 17–19 present the responses of the two-node macro model along its three axes at 25% vertical excitation: case (2).

There is excellent agreement across the three codes, in terms of maxima and minima, for (a) forces (Table 9) given a direction and an intensity of vertical shaking, (b) displacements (Table 10) in the X and Y directions, and (c) displacements in the Z direction for small vertical shaking, namely, cases (1) and (2).

There are significant differences between the OpenSees/LS-DYNA and ABAQUS displacements in the Z direction for case (3) (i.e., 100% vertical acceleration) for which the bearing both buckles in compression and cavitates in tension. The disparities are attributed to the different damping formulations (see Section 6.3.2.3) used for the simulations. In OpenSees and LS-DYNA, damping was assigned to the vertical mode using the Rayleigh formulation, but no damping could be assigned to this mode in ABAQUS. The amplitude of the ABAQUS-predicted displacements associated with bearing buckling and cavitation, which results in a loss of tangent axial stiffness, is much greater than that for OpenSees/LS-DYNA because the response is undamped. Corresponding differences are not seen in the horizontal direction because the energy dissipation is primarily hysteretic and not equivalent viscous.

The difference in the Z displacements for case (3) highlights the importance of using a verified and validated numerical model for a code-to-code comparison, which is challenging for complex nonlinear models because no closed form analytical solutions exist to enable verification.

Table 7
Damping ratios (%) calculated from numerical responses.

Direction	OpenSees			LS-DYNA
	Rayleigh	Mass proportional	Stiffness proportional	Mass proportional
Horizontal	2.003	2.003	2.003	2.005
Vertical	1.999	1.999	1.999	2.009

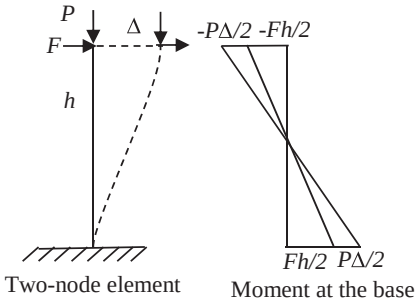

Fig. 15. Bending moments in a two node element.

6.3.3. Order-of-accuracy test

The order-of-accuracy test is the most rigorous code verification activity. The results of the test are very sensitive to small mistakes in the code or deficiencies in the numerical algorithm. It examines the rate at which the discretized numerical solution approaches the exact solution of the mathematical model as mesh discretization parameters are refined. The order of accuracy can be determined as a formal order of accuracy (p) and as an observed order of accuracy ($\hat{p}$). The formal order of accuracy is the theoretical order of convergence of the discrete solution to the exact solution of the mathematical model. The observed order of accuracy is the rate at which computational solution converges to the exact solution of the mathematical model as the mesh size is reduced. The formal order of accuracy is not necessarily the same as the

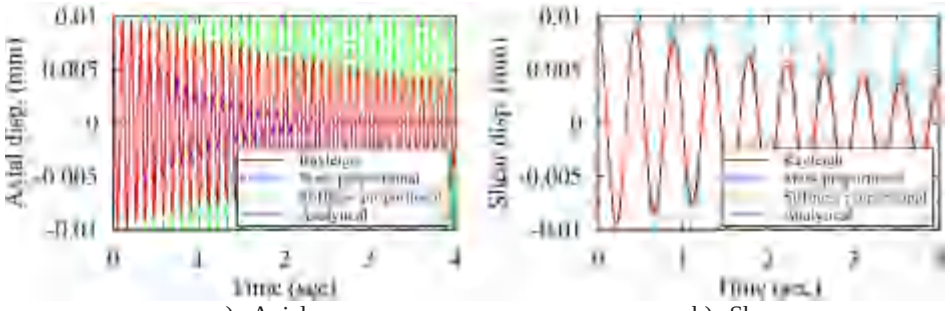

a) Axial b) Shear

Fig. 14. Free-vibration response of a LR bearing using LS-DYNA, u_o = 0.01 mm, ζ = 2%.

Table 8
Bending moments at the two nodes of the element (N-m).

Calculation source	Node 1	Node 2
Theory	86,506	86,506
LeadRubberX	87,660	87,660
elastomericBearingBoucWen	85,740	85,740
twoNodeLink	86,506	86,506
ABAQUS	88,767	88,767
LS-DYNA	65,880	65,880

observed order of accuracy due to errors associated with the code implementation of the discrete numerical solution. Roy and Oberkampf [35] provide a detailed discussion on calculation of formal and observed orders of accuracy. Three values of the response quantity (u_1, u_2, and u_3) are evaluated for time steps of Δt, $r\Delta t$ and $r^2\Delta t$, respectively, to obtain the observed order of accuracy as:

$$\hat{p} = \frac{\ln\left(\frac{\varepsilon_{r\Delta t}}{\varepsilon_{\Delta t}}\right)}{\ln(r)} = \frac{\ln\left(\frac{\|u_3 - u_2\|}{\|u_2 - u_1\|}\right)}{\ln(r)} \tag{6}$$

The code is considered to be verified if the observed order of accuracy is equal to the formal order of accuracy. The LDR and LR bearings of Fig. 4 and Table 4 are subjected to harmonic acceleration inputs to obtain the variations in the order of accuracy with time step, for linear and nonlinear response in shear. Results are presented in Figs. 20 and 21. For the nonlinear calculations of Fig. 21, the LDR and LR bearings are subjected to different amplitudes of harmonic excitation, 0.1 g and 0.5 g, respectively, to obtain similar displacement responses.

The order of accuracy converges to two and one for linear and nonlinear response, respectively. The linear response of a dynamic system using the Newmark integrator is known to be second order accurate (p = 2). As the observed order of accuracy equals the formal order of accuracy, the code correctness can be confirmed for the numerical models for linear response. The formal order of accuracy is unknown for the nonlinear response because there is no closed form analytical solution. However, the observed order of accuracy converges to a fixed value, which confirms the convergence and the stability of the numerical solution.

The temperature rise in the lead core of the LR bearing is calculated for different values of Δt to estimate the observed orders of accuracy for the linear and nonlinear responses presented in Figs. 20 and 21. Results are presented in Fig. 22.

6.4. Solution verification

Solution verification (also called calculation verification) assesses the accuracy of the discretized numerical solution of a mathematical model that is implemented for computational predictions. Solution verification activities commence only after code verification is completed. The error associated with the numerical model is discussed in the following sections.

6.4.1. Discretization error

One of the largest sources of error is associated with discretization, and it is perhaps the most difficult to estimate. There are numerous methods to estimate discretization error. The Generalized Richardson Exploration (GRE) is used here because of its ease of application. This method is useful when an exact solution to the mathematical model is either unavailable or difficult to evaluate. The five conditions that need to be satisfied for application of this method are [10]:

1. The formal order of accuracy should match the observed order of accuracy.
2. Uniform mesh spacing should be used in the numerical model.
3. Discretization should be refined systematically.
4. The obtained solution should be smooth in nature.
5. Other numerical error sources should be small compared to the discretization error.

The GRE uses a systematic discretization refinement to obtain a higher order estimate ($p + 1$ order accurate) of the exact solution to the mathematical model, which can be used in place of the exact solution to obtain error estimates. The higher order estimate, $\bar{u}$, is obtained as:

$$\bar{u} = u_{\Delta t} + \frac{u_{\Delta t} - u_{r\Delta t}}{r^p - 1} \tag{7}$$

If the five conditions for the application of Richardson Exploration Method are satisfied, then $\bar{u}$ calculated in the asymptotic zone of the discretized numerical solution can replace $\tilde{u}$. The percentage discretization error is given as:

$$\%\varepsilon_{\Delta t} = \frac{u_{\Delta t} - \bar{u}}{\bar{u}} \times 100\% = \frac{u_{r\Delta t} - u_{\Delta t}}{u_{\Delta t} r^p - u_{r\Delta t}} \times 100\% \tag{8}$$

The observed orders of accuracy of two and one are used to calculate the discretization errors for linear and nonlinear response, respectively. The value of the refinement ratio r is 2.

The analysis cases of Figs. 20 and 21 are repeated to calculate responses at different time steps. The LDR and LR bearings are subjected to $a_g = 0.001\text{gsin}(\pi t)$ for linear response, and $a_g = 0.1\text{gsin}(\pi t)$ and $0.5\text{gsin}(\pi t)$ for nonlinear response, respectively, as noted previously. The variation in discretization error in shear displacement with time step is presented in Fig. 23. The shear force-displacement loops for the LDR and LR bearings obtained using different time steps are presented in Fig. 24. The reduction in the discretization error with time step indicates a monotonic convergence of the solution. The discretization error and the variation of the temperature rise in the lead core, for different time steps, are presented in Figs. 25 and 26, respectively. The asymptotic zone of solution for shear force and temperature is obtained for time steps smaller than 0.005 s.

An observed order of accuracy of 1 was assumed in the absence of a

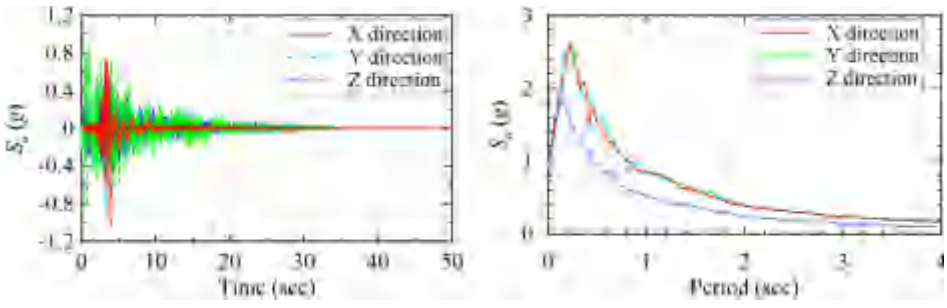

a) Acceleration histories b) Response spectra

Fig. 16. Ground motions used for seismic response-history analysis.

Table 9
Peak force in the two-node macro model for different intensities of vertical excitation.

Vertical excitation	X force (kN)			Y force (kN)			Z force (kN)[a]		
	OpenSees	ABAQUS	LS-DYNA	OpenSees	ABAQUS	LS-DYNA	OpenSees	ABAQUS	LS-DYNA
0	385	392	388	426	428	432	(−1509, −1366)	(−1533, −1345)	(−1533, −1350)
$0.25a_g$	409	411	432	454	453	459	(−2693, 17)	(−2714, 23)	(−2848, 165)
a_g	423	452	452	479	481	489	(−5338, 540)	(−5190, 550)	(−5074, 568)

[a] Positive force is tensile.

Table 10
Peak displacement of the two-node macro model for different intensities of vertical excitation.

Vertical excitation	X displacement (mm)			Y displacement (mm)			Z displacement (mm)[a]		
	OpenSees	ABAQUS	LS-DYNA	OpenSees	ABAQUS	LS-DYNA	OpenSees	ABAQUS	LS-DYNA
0	208	220	217	233	242	241	(−5, −3)	(−6, −3)	(−4, −3)
$0.25a_g$	215	221	220	243	243	242	(−8, 0)	(−8, 0)	(−6, 0)
a_g	219	230	225	253	254	260	(−24, 9)	(−167, 90)	(−19, 12)

[a] Positive displacement is tensile.

formal order of accuracy for the calculation of the discretization errors in the axial and shear response for the nonlinear analysis. If the observed order of accuracy is higher than the formal order of accuracy, the discretization error obtained using the observed order of accuracy provides an unconservative estimate.

6.4.2. Integrators

Integrators are the time stepping procedures that advance the state of analysis from time t to $t + \Delta t$. An integrator determines the matrices in the system of equations $Ax = B$. The isolator user elements are developed for implicit integrators in OpenSees and ABAQUS, but can only be used with an explicit integrator in LS-DYNA. The Newmark and Hilber-Hughes-Taylor (HHT) implicit integrators are available in OpenSees and ABAQUS. A modified Central Difference scheme is used by LS-DYNA. Each of these time-stepping schemes is associated with errors. The stability and the accuracy of the results obtained using these time-stepping schemes depend on the chosen integration parameters.

The Newmark family of integrators are given by the following equations [36]:

$$R_{t+\Delta t} = F^{ext}_{t+\Delta t} - M\ddot{u}_{t+\Delta t} - C\dot{u}_{t+\Delta t} + F^{\text{int}}(u_{t+\Delta t}) \tag{9}$$

$$\dot{u}_{t+\Delta t} = \dot{u}_t + [(1-\gamma)\Delta t]\ddot{u}_{t+\Delta t} + (\gamma\Delta t)\ddot{u}_{t+\Delta t} \tag{10}$$

$$u_{t+\Delta t} = u_t + (\Delta t)\dot{u}_t + [(0.5-\beta)(\Delta t)^2]\ddot{u}_t + [\beta(\Delta t)^2]\ddot{u}_{t+\Delta t} \tag{11}$$

where R is the residual vector, F is the nodal force vector, M and C are the mass and stiffness matrices, u is displacement and γ and β are the Newmark integration parameters. The stability and accuracy of response depends on parameters γ and β. Two special cases of Newmark integrators are: (1) Newmark Average Acceleration, and (2) Newmark Linear Acceleration.

The HHT integration scheme is an extension of the Newmark method and allows for energy dissipation. The evolution of $\dot{u}$ and u in Eqs. (10) and (11) is identical to the Newmark method but a different residual equation is used:

$$R_{t+\alpha\Delta t} = F^{ext}_{t+\alpha\Delta t} - M\ddot{u}_{t+\alpha\Delta t} - C\dot{u}_{t+\alpha\Delta t} + F^{\text{int}}(u_{t+\alpha\Delta t}) \tag{12}$$

where the displacements and velocities between the time steps are given by:

$$u_{t+\alpha\Delta t} = (1-\alpha)u_t + \alpha u_{t+\Delta t} \tag{13}$$

$$\dot{u}_{t+\alpha\Delta t} = (1-\alpha)\dot{u}_t + \alpha\dot{u}_{t+\Delta t} \tag{14}$$

Integrators and their stability conditions are presented in Table 11, where T_n is the fundamental period of the SDOF system. The stability conditions are applicable only for linear problems. The stability of these methods over a wide range of nonlinear problems is not guaranteed.

The integrator chosen for a dynamic analysis can artificially alter the natural periods of a structure and introduce numerical damping, depending on the values assigned to its parameters and the selected time step. The consequent errors in response should be understood, quantified and ideally eliminated, as described below.

The properties of the LDR5 bearing of Warn [27], as given in Table 4, are used for the element connecting the two nodes. The mass is back calculated from the assumed value of the time period in the horizontal direction. The system is undamped. A horizontal displacement of 1 mm is imposed at Node 2, which is then released to vibrate freely. (The shearing displacement at yield is assumed to be 7 mm for the LDR bearing and so the free vibration response is elastic.) OpenSees accommodates all of the

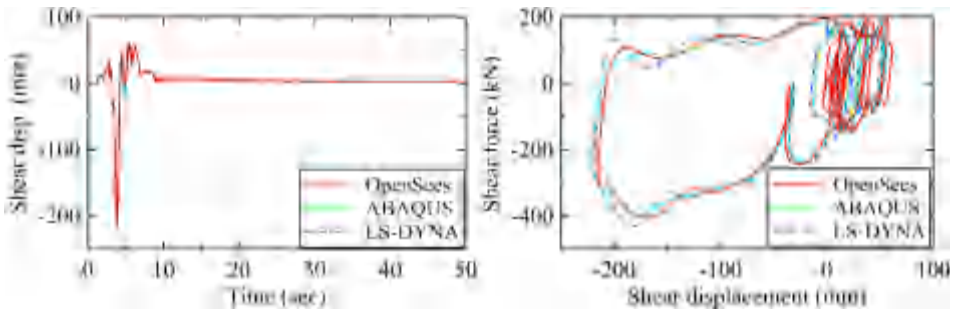

a) Displacement history b) Force-displacement response

Fig. 17. Seismic response of the two-node macro model, case (2), X direction.

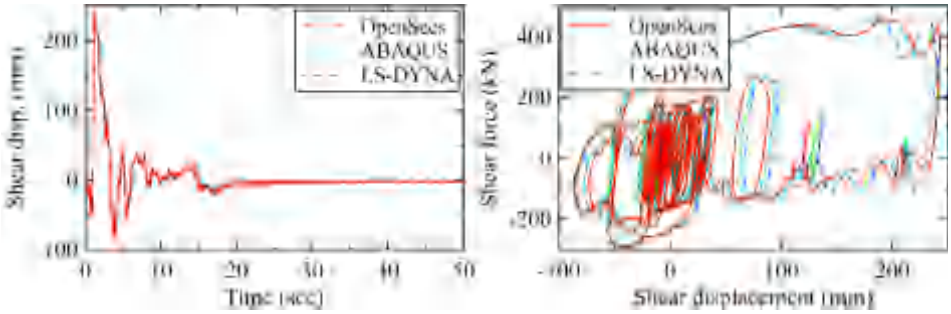

a) Displacement history b) Force-displacement response

Fig. 18. Seismic response of the two-node macro model, case (2), Y direction.

implicit integrators introduced above and so is used to compute responses. For the elastic displacements considered here, the conclusions obtained for ElastomericX are also applicable to LeadRubberX.

The last four integrators listed in Table 11 are used to study the free-vibration response of the two-node macro model for the 1 mm initial displacement of Node 2. Fig. 27 presents the first 5 s of the lateral displacement response of Node 2 for a time step of $\Delta t/T_n = 0.1$ (Δt = 0.2 s, T_n = 2 s). The use of the central difference integrator reduces the period whereas the implicit integrators increase the period, all with respect to the exact value of 2 s. The change in period vanishes for all of the integrators for small values of $\Delta t/T_n$; for $\Delta t/T_n = 0.01$, there is no change in period. Energy dissipation (or damping) is evident in Fig. 27. Fig. 28 presents the equivalent viscous damping ratio (or numerical damping) calculated from the data of Fig. 27 using the logarithmic decrement method. The amount of damping is a function of the chosen integrator and the time step. The smaller the time step, the smaller the numerical damping, with the greatest numerical damping at the larger time steps associated with the HHT integrator. Analyses performed for a range of natural period between 1 and 4 s show similar trends.

7. Validation

7.1. Introduction

The validation process assesses the accuracy with which a mathematical model represents the physical reality for its intended use. Experiments are considered the best available representation of reality. Existing experimental data cannot be used if it inadequately represents the intended use of a model. Experiments are performed simulating the initial and boundary conditions, material properties and applied loads as closely as possible to the model's intended use, while also characterizing the anomalies where present and quantifying the uncertainties in measurements. The outcomes of these specifically designed experiments are compared with predictions using the verified computational models to assess their accuracy. These are termed validation experiments. The primary goal of a validation experiment is to assess the predictive capability of the model by comparing computational results to the experimental outcomes for the response quantities of interest. For validation activities, three conditions must be satisfied:

1. The model is clearly defined, including the reality of interest, its intended use and the response quantities of interest.
2. A verified computational model is used.
3. The uncertainties in the experimental outcomes are quantified.

The scope and intended use of the mathematical models of elastomeric bearing were defined in Table 2. The computational models were verified in the previous section. A plan for experimental validation is developed here based on the PIRT presented in Table 3 and sensitivity analyses. The sources of error (e.g., unknown parameters) in the mathematical model are identified. The goal of a validation experiment is to investigate the characteristics of the mathematical model that are expected to significantly affect the response quantities of interest.

Validation is only concerned with the accuracy of the mathematical model and not its implementation, which are represented here by the isolator elements in OpenSees, ABAQUS, LS-DYNA. Any of the verified computational models can be used to validate mathematical model. The isolator elements in OpenSees are used here to compare computational results with experimental data.

7.2. Sensitivity analysis

A sensitivity analysis of the model was performed by Kumar et al. [4] to identify parameters and phenomena that significantly affected the response quantities of interest. It also assisted in deciding on the behaviors of elastomeric bearings that should be investigated through validation experiments.

The cavitation parameters are determined using experimental data and are expected to have high uncertainty. The tensile response of an elastomeric bearing is more sensitive to the value of cavitation parameter, k, than the damage index, ϕ_{max}, and the strength degradation parameter, a_c. A validation experiment is required to assess the

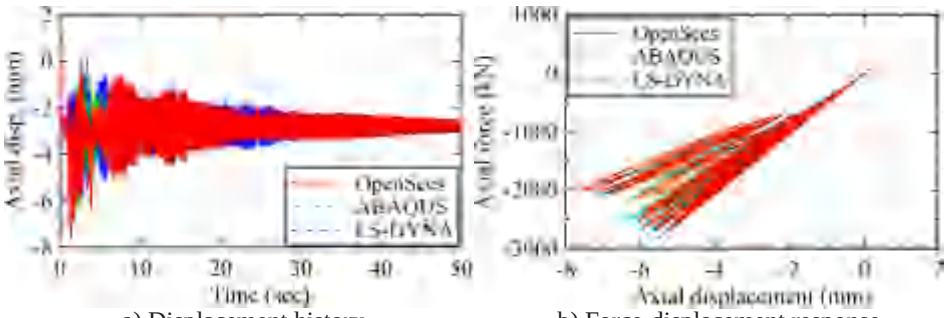

a) Displacement history b) Force-displacement response

Fig. 19. Seismic response of the two-node macro model, case (2), Z direction.

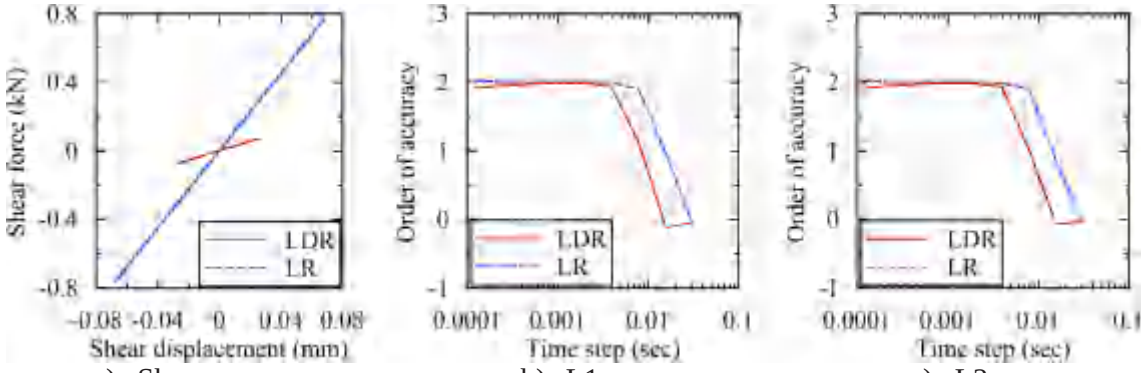

Fig. 20. Order of accuracy for linear response, a_g = 0.001gsin(πt).

predictive capability of the computational model with these cavitation parameters. If the model shows good agreement with the results obtained from the validation experiments, the elastomeric bearing model is considered to be validated. If the numerical predictions differ from the experimental results by an amount greater than the accuracy criteria, two options can be considered:

1. Refine the model using new data obtained from validation experiments, which involves calibration to update cavitation parameters and change any underlying assumption that is not found appropriate based on information obtained from the validation experiment, and then repeat the validation activities with a new set of experiments and the updated model.
2. Restrict the use of model to the conditions for which it satisfies the accuracy criteria.

The chosen option will depend on available resources and the risk associated with the use of a model to predict the outcome of an event.

7.3. Calibration using past experiments

The ability of the verified computational model to predict the response of an elastomeric bearing in shear is investigated through a comparison with available test data.

The models are validated for tensile behavior using three sets of data from past experiments, as shown in Fig. 29. The cavitation parameter and the damage index were obtained by calibration of the mathematical model with experimental data. Information on the bearings used for calibration and the values of k, a_c, and ϕ_{max} are presented in Table 12.

The thermodynamic parameters of lead used in LR bearings are known and do not require calibration with experimental data. Available test data can be used for validation of the mathematical model used to describe the shear behavior of an elastomeric bearing. Computational results and experimental data [21] for the LR bearing in the horizontal direction are presented in Fig. 30, and they agree well.

7.4. Validation experiments

The scope and intended use of the mathematical models of an elastomeric bearing are listed in Table 3. The computational models were verified in the previous section. An experimental plan is developed based on the PIRT presented in Table 3 and experiments are conducted to validate the mathematical model in tension. A detailed description of the experimental set up and experimental results are presented in Kumar et al. [38]. Filtering techniques are employed to remove noise from the data. Redundant measurements of important response quantities are obtained. Additional details on the tools and techniques used to address experimental errors are presented in Kumar et al. [39].

The mathematical model of the mechanical behavior of an elastomeric bearing in tension is based on observations from experiments. A phenomenological formulation was proposed by Kumar et al. [4] to capture this behavior. The model uses three parameters to capture behavior under cyclic tensile loading. The following assumptions are investigated for this model:

1. Cavitation strength decreases (damage increases) with increasing values of tensile strain amplitude of each cycle.
2. No additional damage is observed if the tensile strain is less than its prior maximum value.
3. If the prior maximum value of tensile strain is exceeded, the formation of new cavities leads to additional damage, and the cavitation strength is further decreased.
4. Cavitation strength converges to a minimum value.

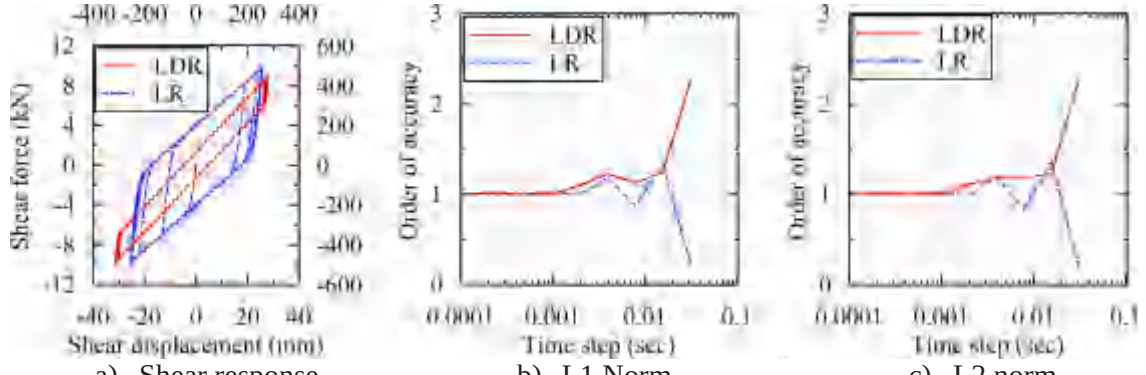

Fig. 21. Order of accuracy for nonlinear response, a_g = 0.1gsin(πt) for the LDR bearing, a_g = 0.5gsin(πt) for the LR bearing).

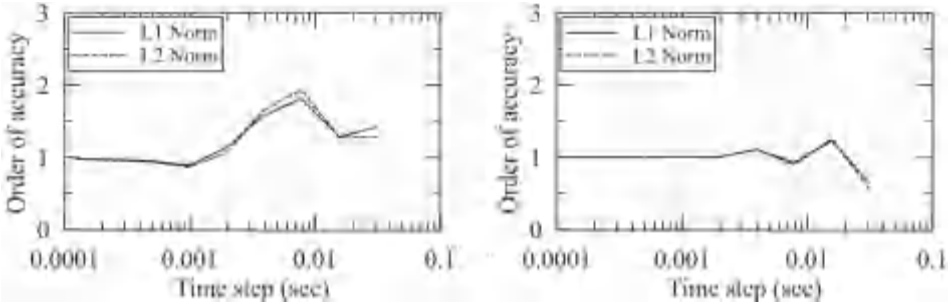

a) Linear b) Nonlinear

Fig. 22. Observed order of accuracy for temperature rise in the lead core of the LR bearing, $a_g = 0.5g\sin(\pi t)$.

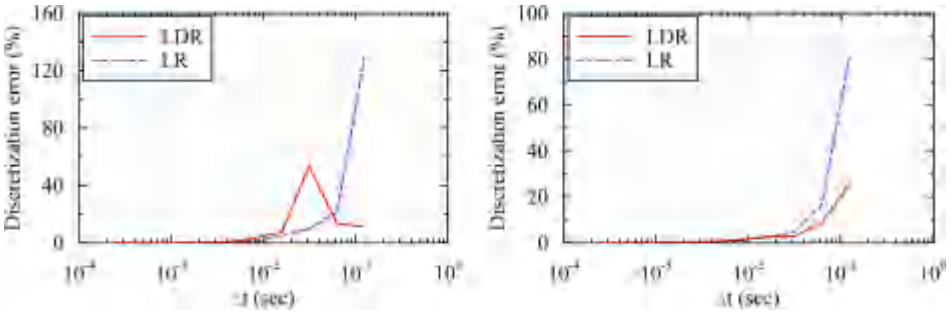

a) Linear shear response b) Nonlinear shear response

Fig. 23. Discretization error in the peak shear force.

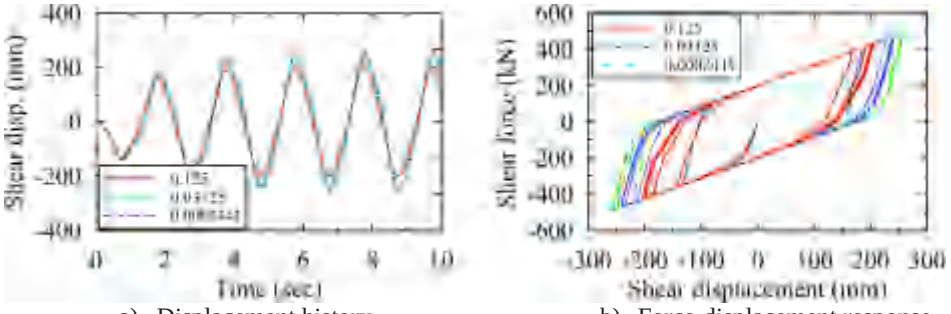

a) Displacement history b) Force-displacement response

Fig. 24. Force-displacement nonlinear response in the horizontal direction, LR bearing, $a_g = 0.5g\sin(\pi t)$, varying time step.

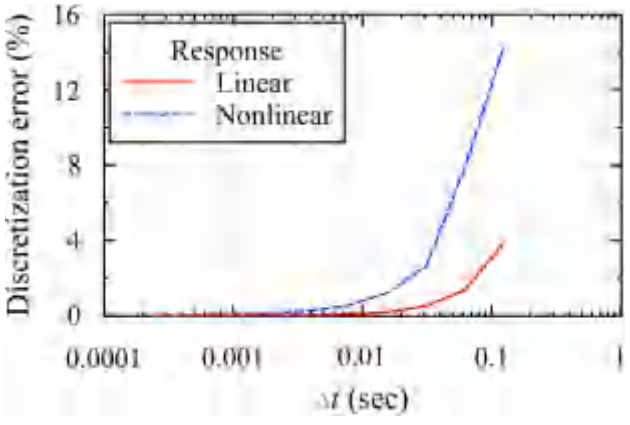

Fig. 25. Discretization error in temperature.

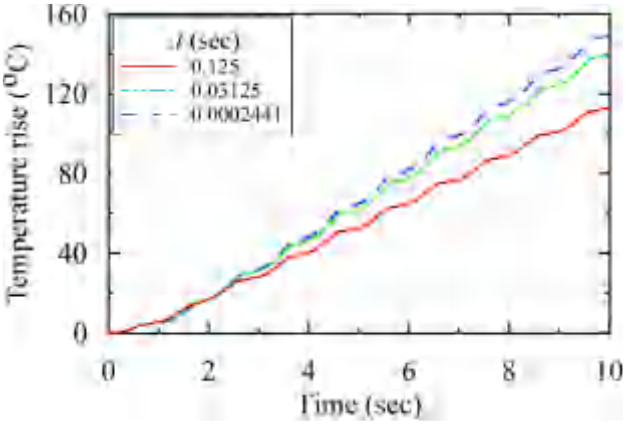

Fig. 26. Temperature increase in the lead core, LR bearing, nonlinear response.

Table 11
Stability requirements for different integrators.

Integrator	Parameters	Stability condition
Newmark (general)	$\beta \geqslant \gamma/2 \geqslant 1/4$	Unconditionally stable
Newmark Average Acceleration	$\gamma = 1/2, \beta = 1/4$	Unconditionally stable
Newmark Linear Acceleration	$\gamma = 1/2, \beta = 1/6$	$\Delta t \leqslant 0.55T_n$
Hilber-Hughes-Taylor (HHT)	$2/3 \leqslant \alpha \leqslant 1$	Unconditionally stable
Central Difference	–	$\Delta t \leqslant 0.318T_n$

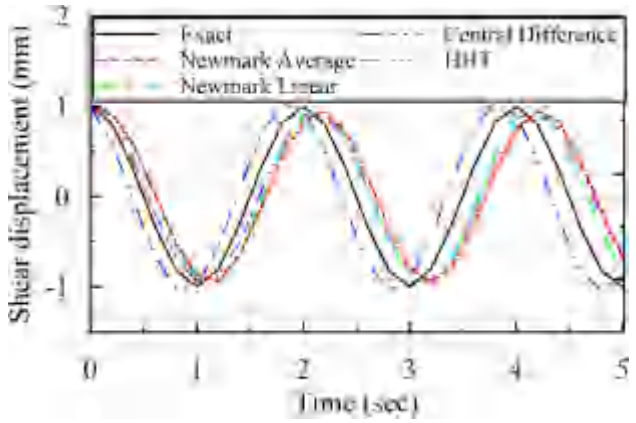

Fig. 27. Shear displacement response of a LDR bearing, u_o = 1 mm, $\Delta t/T_n$ = 0.1.

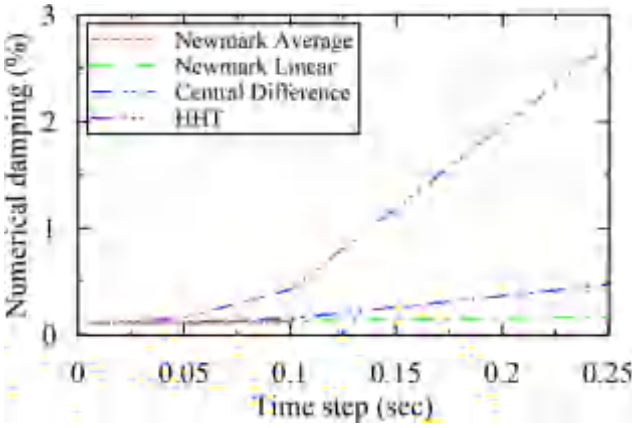

Fig. 28. Variation of numerical damping with time step, u_o = 1 mm, T_n = 2 s.

Table 12
Properties of bearings used for comparing experimental results and numerical predictions.

	Constantinou et al. [15]	Iwabe et al. [37]	Warn [27]
Diameter, mm	250	500	164
Shape factor, S	9.8	33	10.2
k	60	15	20
a_c	1.0	1.0	1.0
ϕ_{max}	0.75	0.75	0.75

A comparison of the experimental behavior and numerical results obtained using the phenomenological model described in Kumar et al. [4] is presented in Fig. 31 for eight of the sixteen tested bearings, where F/F_c is the tensile force normalized by the cavitation strength. The values of the parameters used for the tensile model are: cavitation parameter, k = 20; strength degradation parameter, a = 1.0; and damage index, ϕ_{max} = 0.9. A detailed discussion of experiments is presented in Kumar et al. [38].

Numerical results show reasonable agreement with experimental behavior based on a visual comparison of data. Differences are observed in a few cases between the behaviors shown in Fig. 31 and those observed from past experiments (e.g., Iwabe et al. [37], Kato et al. [40], Warn [27]). It has been observed in previous experimental studies that if the tensile strain exceeds the prior maximum value, the prior maximum value of the tensile force is recovered, and subsequently, tensile force increases with tensile strain. However, force reduction is observed between consecutive cycles for a few of the bearings tested here, and the tensile force is not recovered after the tensile strain exceeds the prior maximum value. The reduction in force might be due to initiation of tensile failure. It is difficult to locate the precise point of failure on the load-deformation curve up to which the phenomenological model can be applied. A consistent failure strain in tension is not observed across all the bearings. The tensile strain capacities of these bearings are smaller than those reported by others (e.g., Iwabe et al. [37], Kato et al. [40], Warn [27], Clark [41]).

8. Summary and conclusions

Advanced mathematical models of elastomeric seismic isolation bearings, namely the low damping rubber bearing (LDR) and the lead-rubber (LR) bearing, were implemented in OpenSees, ABAQUS and LS-DYNA to enable cross-platform usage. The implementation, including input arguments and capability and limitations of these user elements are presented. These models are verified and validated per ASME best practices and guidelines. A verification plan is prepared for the computational model of elastomeric bearings. The computational model is represented here by user elements of LR and LDR bearings implemented in OpenSees, ABAQUS and LS-DYNA. Several sets of analyses are

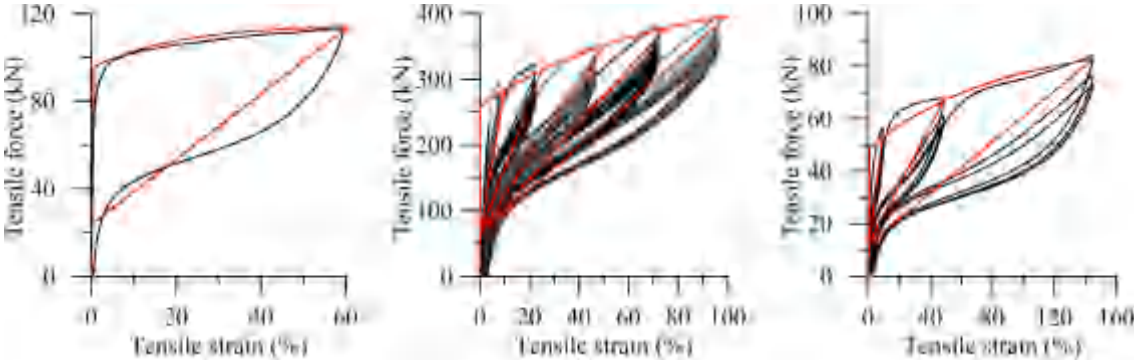

(a) Constantinou *et al.* [15] (b) Iwabe *et al.* [37] (c) Warn [27]

Fig. 29. Experimental and numerical results for LDR bearings in tension [4].

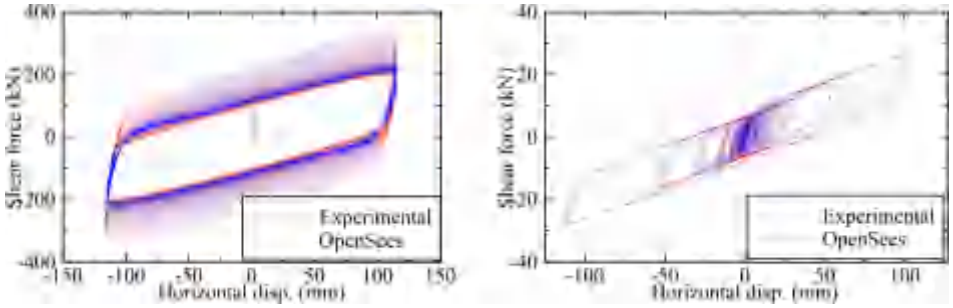

a) Harmonic loading b) Random excitation

Fig. 30. Shear force-displacement behavior of a LR bearing under harmonic loading.

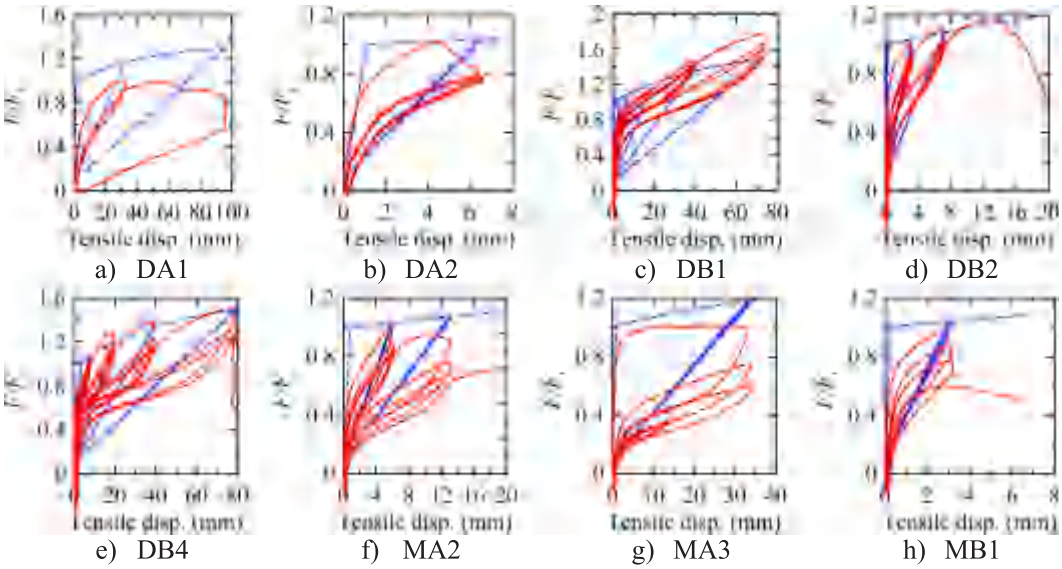

a) DA1 b) DA2 c) DB1 d) DB2

e) DB4 f) MA2 g) MA3 h) MB1

Fig. 31. Validation of the mathematical model in tension, normalized force vs. displacement.

performed using these user elements to identify and quantify sources of error. Where possible, errors are eliminated by removing their sources or minimized by sensitivity analyses. All verification activities are performed using the ElastomericX and LeadRubberX user elements in OpenSees. Verification of the isolator models in ABAQUS and LS-DYNA is limited to a comprehensive code-to-code verification.

The most important conclusions from these verification activities are:

1. The component of the mathematical model that contributes most to the error is heating of the lead core in the LR bearing.
2. Code-to-code verification shows good agreement between OpenSees, ABAQUS and LS-DYNA, with the error in peak response of less than 5%.
3. OpenSees allows accurate modeling of Rayleigh, mass-proportional, and stiffness-proportional damping with the isolator element. Only mass-proportional damping formulation can be used for the isolator element in LS-DYNA. None of three damping formulations can be used with a user subroutine in ABAQUS.
4. The observed order of accuracy is equal to the formal order of accuracy of the numerical model for linear response of the LDR and LR isolators.
5. The asymptotic zone of solution for shear force and temperature is obtained for time steps less than 0.005 s, beyond which discretization error in the shear displacement is less than 1%.
6. For values of the ratio $\Delta t/T_n$ (analysis time step/time period) less than 0.1, no significant numerical energy dissipation is observed.
7. The Newmark Average Acceleration integrator provides the least numerical damping of those investigated here.

The verified models are first calibrated using experimental data to determine unknown model parameters. The mathematical models are then validated using data from a series of experiments to characterize the behavior of elastomeric bearings in tension and tension/shear. Sixteen low damping rubber bearings from two manufacturers, with similar geometric properties but different shear moduli, are tested under various loading conditions to identify those factors that affect cavitation in an elastomeric bearing. The effect of cavitation on the shear and axial properties of elastomeric bearings is investigated by performing post-cavitation tests. The test data are used to validate a phenomenological model of an elastomeric bearing in tension.

The key conclusions of the validation experiments are:

1. The mathematical model of an elastomeric bearing in tension shows reasonable agreement with the behavior observed from experiments.
2. The linear behavior in tension assumed for elastomeric bearings, and implemented in commercial software packages for the analysis of structures, is only valid up to the point of cavitation and cannot capture the post-cavitation behavior of an elastomeric bearing. Importantly, the linear stiffness in tension is a function of lateral displacement.
3. Validation experiments must be independent of calibration tests used to estimate the model parameters to ensure accurate quantification of modeling error.
4. The large differences in tensile behaviors, including stiffness and cavitation pressure, observed from tests of bearings from two manufacturers, is attributed to bearing fabrication and manufacturing quality control.

The limitations of modeling techniques used for structural and earthquake engineering analysis should be acknowledged. It is not always feasible to include and V + V all possible features of a model. A practical V + V plan is adopted here. Accordingly, the scope of the V + V activities is restricted to the model's intended use and the response quantities of interest. These key conclusions are expected to be valid for bearings of a shape and size typically used for seismic isolation applications.

Acknowledgements

This research project was supported by a grant to MCEER from the United States Nuclear Regulatory Commission (USNRC) and the Lawrence Berkeley National Laboratory (LBNL). This financial support is gratefully acknowledged. The authors thank Dr. Michael Constantinou of the University at Buffalo and Dr. Robert Budnitz of LBNL for their input into the V + V activities, and to former University at Buffalo graduate students Dr. Ioannis Kalpakidis of Energo Engineering and Dr. Gordon Warn of Penn State University for providing test data on elastomeric bearings. Authors are also thankful to Dr. Yuli Huang of ARUP, Inc, who helped with the implementation of the isolator UMAT in LS-DYNA.

Appendix A. Supplementary material

Supplementary data associated with this article can be found, in the online version, at https://doi.org/10.1016/j.engstruct.2018.08.047.

References

[1] Kato H, Mori T, Murota N, Suzuki S. A new hysteresis model based on an integral type deformation-history for elastomeric seismic isolation bearings. Proceedings: 15th World Conference in Earthquake Engineering, Lisbon, Portugal; 2012.
[2] Ryan KL, Kelly JM, Chopra AK. Nonlinear model for lead-rubber bearings including axial-load effects. J Eng Mech 2005;131(12):1270–8.
[3] Yamamoto S, Kikuchi M, Ueda M, Aiken ID. A mechanical model for elastomeric seismic isolation bearings including the influence of axial load. Earthquake Eng Struct Dyn 2009;38(2):157–80.
[4] Kumar M, Whittaker A, Constantinou M. An advanced numerical model of elastomeric seismic isolation bearings. Earthquake Eng Struct Dyn 2014;43(13):1955–74.
[5] CSI. SAP2000 user's manual–version 11.0. Berkeley, CA: Computer & Structures Inc.; 2007.
[6] CSI. Computer Program PERFORM-3D. Berkeley, CA: Computer & Structures Inc.; 2006.
[7] LSTC. Computer Program LS-DYNA. Livermore, CA: Livermore Software Technology Corporation; 2012.
[8] Computer Program ABAQUS/CAE. Dassault Systèmes. Providence, RI; 2010.
[9] American Society of Mechanical Engineers (ASME). Guide for verification and validation in computational solid mechanics. ASME V&V 10–2006, New York, NY; 2006.
[10] Oberkampf WL, Roy CJ. Verification and validation in scientific computing. Cambridge: Cambridge University Press; 2010.
[11] Oberkampf WL, Trucano TG, Hirsch C. Verification, validation, and predictive capability in computational engineering and physics. Appl Mech Rev 2004;57(1–6):345–84.
[12] Thacker BH, Doebling SW, Hemez FM, Anderson MC, Pepin JE, Rodriguez, EA. Concepts of model verification and validation. Los Alamos National Lab., Los Alamos, NM (US); 2004.
[13] Roache PJ. Verification and validation in computational science and engineering. Albuquerque, NM: Hermosa Publications; 1998.
[14] Kammerer AM, Whittaker AS, Constantinou MC. Technical considerations for seismic isolation of nuclear facilities. NUREG-, United States Nuclear Regulatory Commission, Washington, DC; 2018.
[15] Constantinou MC, Whittaker AS, Kalpakidis I, Fenz DM, Warn GP, 2007. Performance of seismic isolation hardware under service and seismic loading. Technical Report MCEER-07-0012, University at Buffalo, State University of New York, Buffalo, NY.
[16] Koh CG, Kelly JM. Effects of axial load on elastomeric isolation bearings. Technical Report EERC/UBC-86/12, Earthquake Engineering Research Center, University of California, Berkeley, CA; 1987.
[17] Warn GP, Whittaker AS, Constantinou MC. Vertical stiffness of elastomeric and lead-rubber seismic isolation bearings. J Struct Eng 2007;133(9):1227–36.
[18] Park YJ, Wen YK, Ang AHS. Random vibration of hysteretic systems under bi-directional ground motions. Earthq Eng Struct Dyn 1986;14(4):543–57.
[19] Wen Y-K. Method for random vibration of hysteretic systems. J Eng Mech Div 1976;102(2):249–63.
[20] Nagarajaiah S, Reinhorn AM, Constantinou MC. Nonlinear dynamic analysis of 3-d-base-isolated structures. J Struct Eng 1991;117(7):2035–54.
[21] Kalpakidis IV, Constantinou MC, Whittaker AS. Modeling strength degradation in lead-rubber bearings under earthquake shaking. Earthquake Eng Struct Dyn 2010;39(13):1533–49.
[22] Dassault. Writing user subroutines with ABAQUS. Workshop by Simulia services. Dassault Systèmes, Providence, RI; 2012.
[23] LSTC. LS-DYNA keyword user's manual. Livermore, CA: Livermore Software Technology Corporation; 2017.
[24] Kumar M, Whittaker A, Constantinou M. Response of base-isolated nuclear structures to extreme earthquake shaking. Nucl Eng Des 2015;295:860–74.
[25] Kalpakidis IV, Constantinou MC. Effects of heating on the behavior of lead-rubber bearings. II: Verification of theory. J Struct Eng 2009;135(12):1450–61.
[26] Warn GP, Whittaker AS. A study of the coupled horizontal-vertical behavior of elastomeric and lead-rubber seismic isolation bearings. Technical Report MCEER-06-0011, University at Buffalo, State University of New York, Buffalo, NY; 2006.
[27] Warn GP. The coupled horizontal-vertical response of elastomeric and lead-rubber seismic isolation bearings. Ph.D. Dissertation. University at Buffalo, State University of New York, Buffalo, NY; 2006.
[28] McKenna F, Fenves G, Scott M. OpenSees: Open System for Earthquake Engineering Simulation. Pacific Earthquake Engineering Research Center, University of California, Berkeley, CA; 2006 < http://opensees.berkeley.edu > .
[29] Trucano TG, Pilch M, Oberkampf WL. On the role of code comparisons in verification and validation. Sandia Natl Lab 2003;SAND2003-2752.
[30] Dassault. ABAQUS 6.10 verification manual. Abaqus 6.10 Documentation. Dassault Systèmes, Providence, RI; 2010.
[31] Dassault. ABAQUS 6.10 benchmarks manual. Abaqus 6.10 Documentation. Dassault Systèmes, Providence, RI; 2010.
[32] American Society of Mechanical Engineers (ASME). Quality assurance requirements for nuclear facility applications. ASME NQA-1-2015, New York, NY; 2015.
[33] Chopra AK, McKenna F. Modeling viscous damping in nonlinear response history analysis of buildings for earthquake excitation. Earthq Eng Struct Dyn 2015:193–211.
[34] Kumar M, Whittaker AS, Constantinou MC. Seismic isolation of nuclear power plants using sliding bearings. Technical Report MCEER-15-0006, University at Buffalo, State University of New York, Buffalo, NY; 2015.
[35] Roy CJ, Oberkampf WL. A comprehensive framework for verification, validation, and uncertainty quantification in scientific computing. Comput Methods Appl Mech Eng 2011;200(25–28):2131–44.
[36] Chopra AK. Dynamics of structures: Theory and applications to earthquake engineering. Prentice Hall, NJ, USA; 2007.
[37] Iwabe N, Takayama M, Kani N, Wada A. Experimental study on the effect of tension for rubber bearings. In: Proceedings: 12th World Conference on Earthquake Engineering, New Zealand; 2000.
[38] Kumar M, Whittaker A, Constantinou M. Experimental investigation of cavitation in elastomeric seismic isolation bearings. Eng Struct 2015;101:290–305.
[39] Kumar M, Whittaker AS, Constantinou MC. Seismic isolation of nuclear power plants using elastomeric bearings. Technical Report MCEER-15-0008, University at Buffalo, State University of New York, Buffalo, NY; 2015.
[40] Kato R, Oka K, Takayama M. The tensile tests of natural rubber bearings focused on the effect of the steel flange plates. In: Proceedings: Pressure Vessels and Piping Conference, American Society of Mechanical Engineers, Cleveland, OH; 2003, p. 81–88.
[41] Clark PW. Experimental studies of the ultimate behavior of seismically-isolated structures. Ph.D. Dissertation. University of California, Berkeley, CA; 1996.